The Golgi complex is a regulatory hub for homologous recombination-mediated DNA repair.

George Galea[1*], Karolina Kuodyte[1,2], Muzamil M. Khan[1,3], Peter Thul[4], Beate Neumann[5], Emma Lundberg[4,6,7], Rainer Pepperkok[1,3,5*]

[1]Cell Biology and Biophysics Unit, European Molecular Biology Laboratory (EMBL), 69117 Heidelberg, Germany
[2]Collaboration for joint PhD degree between EMBL and Heidelberg University, Faculty of Biosciences
[3]Translational Lung Research Center Heidelberg, German Center for Lung Research, Heidelberg, Germany
[4]Science for Life Laboratory, School of Engineering Sciences in Chemistry, Biotechnology and Health, KTH - Royal Institute of Technology, Stockholm, 17121, Sweden.
[5]Advanced Light Microscopy Facility, EMBL, Heidelberg, 69117, Heidelberg, Germany
[6]Department of Bioengineering, Stanford University, Stanford, CA 94305, USA
[7]Department of Pathology, Stanford University, Stanford, CA 94305, USA

*corresponding authors
e-mail: george.galea@embl.de; rainer.pepperkok@embl.org

Abstract

The Golgi complex has long been recognised as an important homeostasis hub, where a multitude of signalling pathways and essential cellular processes intersect. Yet its communication with the cell nucleus remains largely unexplored. To this end, we have analysed genome-scale localisation data of the Human Protein Atlas which revealed an unexpected high number of Golgi and nuclear dual-localisation proteins and several pathways including surprising DNA repair. Amongst these proteins we found RAD51C, a regulatory Homologous Recombination (HR) repair protein, that localises to the Golgi and in response to double-strand DNA breaks, the Golgi protein population of RAD51C redistributes to form DNA repair foci. Depletion of the Golgin Giantin induces the redistribution of the RAD51C Golgi pool to form nuclear foci, independent of DNA damage induction. Concurrent with a significant increase in genomic instability and inhibition of HR signalling regulators. Altogether, we present evidence for a novel pathway where the Golgi is a central regulatory hub for HR-mediated DNA repair and potentially other repair pathways.

Introduction

Eukaryotic cells have evolved a highly specialised and coordinated array of membrane-bounded organelles. This compartmentalisation allows the segregation of biochemical reactions, ensuring that they are carried out with the highest specificity and efficiency. However, organelles do not function in isolation but rely on the continual exchange of lipids, proteins and signalling cues to maintain cellular homeostasis. At the centre of this cross-coordination of subcellular transport and signalling pathways lies the Golgi complex. Thus, contributing well beyond its classical roles of membrane trafficking, and post-translational modification but rather acting as a regulatory hub with numerous cellular processes intersecting at this organelle such as autophagy, mitosis, growth signalling, cytoskeletal and energy status regulation[1,2]. Various perturbations to the Golgi architecture and mutations of its constituents have been associated with a wide array of human diseases such as neurodegenerative diseases, and cancer, amongst many others[3–6]. Even though we have a clearer picture of the Golgi's interactions and regulatory functions, its communication with the cell nucleus remains largely unexplored.

Emerging themes have started to illustrate the relationship between the Golgi and nuclear compartment, with multilocalisation proteins playing a pivotal role. In cholesterol homeostasis and ER stress response, sensing-signalling proteins SREBP and ATF6, respectively, get proteolytic cleaved at the Golgi complex to regulate gene expression through the release of a transcriptionally active amino terminus that makes its way to the nucleus[7,8]. Regulatory Golgi functions are also present at the onset of mitosis, where the organelle undergoes a multi-step fragmentation process that is required for its correct partition into the dividing cells[9]. Inhibition of this disassembly results in cell-cycle arrest and the block of a set of Golgi-localised proteins that perform specific functions during mitosis, such as mitotic spindle formation and regulation of the spindle checkpoint.

Few studies have also hinted at a link between cytoplasmic organelles, genomic stability, and, in turn, cancer, with the Golgi complex emerging as a central theme[10–12]. At a structural level, the Golgi undergoes dramatic morphological changes after the induction of DNA lesions, from ribbon-like perinuclear stack to dispersed fragments[13]. A response requiring the

phosphorylation of the Golgi oncoprotein Golgi phosphoprotein 3 (GOLPH3) by DDR regulator DNA-dependent protein kinase (DNA-PK)[13]. Golgi morphology alterations are also a common feature across a wide variety of cancer types and are often reflected in changes in the distribution of Golgi resident proteins[11,12]. Rearrangement of Golgi glycosyltransferases distribution is not uncommon in cancer cells, resulting in defective glycosylation, a process thought to promote cancer development[11,12,14]. It remains to be seen what are the impacts of these Golgi organisational changes and whether they're part of a response to DNA damage or a cause of carcinogenesis.

Here, we utilise localisation data and antibody resources from the Human Protein Atlas (HPA) project[15] to explore a class of multilocalisation proteins as a systematic strategy to identify key signalling pathways that function between the Golgi and nuclear compartment. In our work, we validate the first example of a network of DNA repair proteins localised to the Golgi complex and furthermore we propose a novel regulatory pathway for DDR control at the Golgi complex, activating Homologous Recombination (HR)-mediated DNA repair through the interaction of RAD51C and Giantin. Our data also suggests that this regulation is not just restricted to HR DNA repair and RAD51C but could extend to other types of DNA repair mechanisms. This work lays the groundwork for opening up an exciting new scientific niche with the potential of identifying novel therapeutic targets.

Results

Antibody-based analysis identifies a network of DNA damage response proteins at the Golgi complex.

To systematically explore possible candidate that link Golgi to nuclear function or vice versa, we shortlisted 329 proteins identified by the Human Protein Atlas (HPA) project[15] to localise at both Golgi-like membranes and the cell nucleus. siRNA mediated validation experiments[16] confirmed the double-localisation of 163 candidates (167 antibodies) (**Supplementary table S1**).

Bioinformatic analysis of these 163 candidates revealed two major pathways, a membrane trafficking and DNA damage response clusters (**Fig. 1a**). These surprising findings prompted us to explore further whether the double localisation represents moonlighting functions or indeed links between DNA Damage Response (DDR) to Golgi function.

RAD51C Golgi population redistributes to the nucleus in response to DNA damage events.

To address this question and gain mechanistic insight into the role of these DDR proteins at the Golgi, we characterised the HR repair protein RAD51C, based on its importance for the regulation of HR DNA repair[17]. The protein is part of the RAD51 recombinase protein family, which is a key active complex in the recombination-mediated repair of Double-Strand DNA Breaks (DSBs)[18,19]. Following the RAD51C localisation validation, we further confirmed these results using other available antibodies in a number of different cell lines (**Fig. 1b; Extended Data Fig. 1a**). We observed (**Fig. 1b**) that endogenous RAD51C was present in a juxta-nuclear compact localisation (**yellow arrow**) that colocalized with the Golgi marker, GM130 and a diffused nuclear distribution with foci present **(white arrow)**. The specificity of the

antibody was tested by the depletion of RAD51C (**Extended Data Fig. 1b-d**). To biochemically validate the subcellular localisation of RAD51C, we isolated nuclear, membrane and cytoplasmic fractions from HeLa Kyoto (HK) protein extracts and probed them for RAD51C presence in each compartment (**Fig. 1c**). The protein was found to be present in all fractions, in agreement with our immunofluorescence data.

Since RAD51C has been reported to be recruited to DNA repair foci upon the introduction of DSBs[20], we induced the formation of these DNA lesions by treating cells with doxorubicin (DOX) and monitored for changes in RAD51C localisation. DOX is a widely used therapeutic that interacts with DNA by intercalation leading to DSBs[21]. Upon the addition of the drug (**Fig. 1d-g**), we observed an overall decrease in RAD51C protein level, with the portion of the RAD51C colocalising with the Golgi marker, GM130 (**yellow arrows**), reducing at a higher rate than in the nuclear compartment. The RAD51C diffused nuclear pattern changed into very distinct nuclear foci (**white arrows**), with this redistribution getting more pronounced with increasing length of DOX treatment (**Fig. 1d**). Analysis of these experiments allowed us to measure the changes in RAD51C levels at both the Golgi (**Fig. 1e**) and the nuclear compartment (**Fig. 1f**), and to calculate a RAD51C Golgi-nuclear distribution ratio (**Fig. 1g**). This ratio provides a robust and quantitatively measure of the RAD51C Golgi-nuclear distribution, despite fluctuations of protein levels. The RAD51C redistribution was further validated by subcellular fractionation (**Extended Data Fig. 1e, f**). Similarly, the total protein level of RAD51C is observed to decrease after 3h treatments, with a much larger reduction in the membrane compartment when compared to the nuclear fraction. In both experiments, the RAD51C distribution ratio is seen to decrease significantly after 3 h DOX treatment in both the immunofluorescence and biochemical assay (**Fig. 1g, Extended Data Fig. 1f).**

To identify a possible mechanism of this RAD51C redistribution from one compartment to another, we introduced DSBs using DOX, while inhibiting the Importin-β-mediated nuclear import, utilising the small peptide inhibitor Importazole (IPZ)[22]. Treatment with IPZ (**Fig. 2a-c, Golgi fraction marked with yellow arrows; nuclear foci marker with white arrows**) inhibited the DOX induced RAD51C localisation pattern change, instead, the majority of the protein population remained colocalizing with the Golgi marker, GM130, and a significant inhibition of RAD51C nuclear foci formation was observed **(Fig. 2a-c)**. A reduction in the overall RAD51C protein level was observed when cells were treated with DOX only, but there was no significant change in the RAD51C distribution pattern when cells were co-treated with IPZ.

Having established that the RAD51C Golgi population responds to DSB-inducing treatments, we sought to test whether the phosphorylation of DDR kinases mediates this redistribution. The three master kinases that are active in response to DNA damage are ataxia-telangiectasia mutated (ATM), Ataxia telangiectasia and Rad3-related (ATR) and DNA-dependent protein kinase (DNA-PK)[23]. We treated cells with phosphorylation inhibitors specific for each kinase and analysed RAD51C redistribution after DOX treatment (**Fig. 2d-f; Golgi fraction marked with yellow arrows; nuclear foci marked with white arrows**). The combination treatment of DOX with the ATM phosphorylation inhibitor, KU55933[24] significantly inhibited the redistribution of RAD51C, with most of the protein population still colocalising with the Golgi marker, GM130 and an inhibition of nuclear foci formation. Whereas the combined treatment of DOX with ATR and DNA-PK phosphorylation inhibitor, VE-821[25] and NU7441[26] respectively, had no apparent impact on the redistribution of RAD51C when compared with cells treated

with DOX only**.** No apparent changes in the RAD51C localisation pattern were observed with the treatment of inhibitors only (**Extended Data Fig. 2**).

To ensure that these observations are a direct result of DSBs and not the drug itself, we next investigated the effects of other DSB-causing drugs[27]: camptothecin (CPT) (**Extended Data Fig. 3a-c**), etoposide (ETO) (**Extended Data Fig. 3d-f**), and mitomycin C (MMC) (**Extended Data Fig. 3g-i**). All treatments caused significant RAD51C distribution from the Golgi to the nuclear compartment. Furthermore, treatment with CPT (**Extended Data Fig. 3a**) led to a change in RAD51C distribution in the nuclear compartment, from a diffused distribution to distinct nuclear foci, while the application of ETO and MMC (**Extended Data Fig. 3d, g**) resulted in an increase in RAD51C nuclear population but with no apparent nuclear foci pattern.

RAD51C Golgi localisation is dependent on the Golgin Giantin.

To identify potential Golgi candidates that could act as membrane anchors for RAD51C, we analysed data from two genome-wide siRNA screens carried out to identify regulators of HR and DDR (**Extended Data Fig. 4a, b**)[28,29]. Interestingly in these works, the Golgin protein family was highlighted as potential candidate genes, where the knockdown of GMAP210 and Giantin lead to a significant reduction in HR repair rates[28] (**Extended Data Fig 4a**), with the depletion of Giantin also leading to a significant inhibition of H2AX phosphorylation, which is important for DDR signalling regulation[29] (**Extended Data Fig 4b**). The Golgin family is composed of predominantly coiled-coil proteins that are anchored to the Golgi membrane by their carboxy terminus and are predicted to adopt an extended conformation that projects into the surrounding cytoplasm. This arrangement is ideal for the capture or tethering of nearby membranes[30] and also could potentially act as a surface that retains DDR proteins, such as RAD51C. Therefore, we tested whether the localization of RAD51C is dependent on these two Golgins (**Fig. 3a-d**). siRNA mediated depletion of GMAP210 and treatment with a control siRNA had no significant effect on RAD51C distribution, whereas the knock-down of the Golgi matrix protein Giantin led to a significant redistribution of RAD51C (**Fig. 3a**). We observed a significant decrease in the colocalization of RAD51C with the Golgi marker (**yellow arrows**), GM130 and a change in protein localisation in the nucleus from a diffused distribution to distinct bright nuclear foci (**white arrows**) (**Fig. 3a**)**.** Quantifications showed a reduction of the RAD51C Golgi population (**Fig. 3b**) with the distribution ratio (**Fig. 3c**) reduced by more than half and the number of RAD51C foci (**Fig. 3d**) increased by more than two-fold upon depletion of Giantin with either siRNAs. While there was no significant difference in either RAD51C Golgi intensity, distribution ratio or foci number (**Fig. 3b-d**) between the GMAP210-depleted and control cells. In light of these results, we next tested whether RAD51C physically interacts or forms a complex with Giantin by performing an immunoprecipitation (IP) assay (**Fig. 3e**). Here, we immunoprecipitated endogenous Giantin, probed for RAD51C and vice versa (**Fig. 3e**). Endogenous Giantin and RAD51C were found to co-immunoprecipitate from HK protein extracts in both conditions.

To gain insight into the nature of RAD51C foci induced by Giantin depletion, we carried out colocalization assays to determine whether these structures contain standard HR markers, phosphorylated H2AX (γ-H2AX) (**Fig. 4a, b**) and phosphorylated ATM (p-ATM) (**Fig. 4c, d**) under physiological conditions. Both proteins are well established markers for DSB repair sites and are important for the recruitment of the HR repair machinery[31]. In cells treated with a

control siRNA, we observed that close to half of the RAD51C nuclear foci were decorated with either y-H2AX or p-ATM (**Fig. 4a, b**; **colocalising foci are denoted with an arrow**), as previously described in literature[31]. RAD51C foci induced by the depletion of Giantin however showed significantly lower colocalization with both markers (**Fig. 4b, d).**

Depletion of Giantin leads to genomic instability and inhibition of DDR signalling

Having tested the requirement of Giantin in the recruitment and localisation of RAD51C, we next assessed whether the redistribution of the HR protein by the depletion of Giantin would have any significant impact on the cells' ability to maintain genomic stability and undergo DNA repair. To gauge the status of the cell genome, we applied the comet assay[32] which provides a measure of fragmented genomic DNA, an indicator of genomic stability (**Fig. 5a, b**). Cells treated with DNA damaging agents or having impaired DNA repair pathways would result in distinctive long comet tails, due to significant amounts of fragmented genomic DNA. In contrast, healthy untreated cells would display shorter or no comet tail. In our experiment (**Fig. 5a, b**), we observed that samples treated with siRNAs against Giantin and RAD51C showed significantly longer comet tails when compared to the control siRNA treatment. Quantifications of the comets (**Fig. 5b**) showed that the knockdown of RAD51C resulted in a 2.5-fold increase in the comet tail length and fluorescence intensity, here quantified as a standard metric known as olive tail moment[33]. Depletion of Giantin using two different siRNAs (siGiantin#1 and siGiantin#2) resulted in 1.8 and 1.6-fold change in the olive tail moment ratio. Next, we validated this effect on genomic stability by measuring the incidence of micronuclei (denoted with white arrows) (**Fig. 5c, d**). We therefore analysed cell populations depleted of Giantin and RAD51C for their occurrence. Our results highlighted a significantly larger percentage of the cell population displayed micronuclei formation and aberrant nuclear structure after the depletion of Giantin and RAD51C when compared to our control samples (**Fig. 5d**).

RAD51C is required for DSB repair by HR and therefore its change in localisation due to Giantin depletion might lead to inhibition of this pathway and activation of the alternative repair system, the Non-Homologous End Joining (NHEJ) repair[34]. To gain insight into the mechanism by which the redistribution of RAD51C leads to a decrease in genomic stability, cells depleted of Giantin were assessed for their ability to phosphorylate and thereby activate well-characterised regulators of HR and NHEJ repair pathways in response to DNA damage (**Fig. 5e, f**). In our negative control, HK cells treated with DOXO and CPT, we observe increased levels of phosphorylated ATM, CHK2, H2AX (**Fig.5e**) and DNA-PK (**Fig. 5f**) in response to the treatment when compared to our solvent control. Cells depleted of the Golgi protein Giantin when treated with DOXO and CPT showed significantly lower levels of phosphorylation of the tested HR DDR proteins, when compared to our control siRNA (**Fig. 5e, f**). Finally, to assess whether this effect is not a result of cell cycle perturbations, we assessed the cell cycle profile of cells depleted of Giantin (**Fig. 5g**), using Fluorescence Activated Cell Sorting (FACS) analysis, where no significant effects were observed.

Discussion

In this study, we have explored how the Golgi complex and the cell nucleus can communicate with each other in a functional manner. Analysis of genome-scale localisation data of the HPA project[15] revealed a surprisingly high number of double-localising Golgi-nuclear proteins and, even more remarkable, a protein cluster of DNA repair proteins. The latter reflecting important

regulatory proteins of various DNA repair pathways (**Fig. 1a**), not only specific for HR-mediated DNA repair but also Non-Homologous End Joining (NHEJ), Mismatch Repair (MMR) and Base Excision DNA Repair (BER), as well as other integral regulators of DNA repair cellular response such as chromatin cohesion, ubiquitination, cell cycle and signalling. To our knowledge, these findings present the first report of DNA repair protein cluster to localise to the Golgi complex. Exploring in more detail one of the major DNA repair proteins identified, RAD51C, confirmed a functional involvement of its Golgi population in the regulation of HR-mediated DNA repair.

Here, we propose a model (**Fig. 6**) where the cytoplasmic tail of Giantin anchors RAD51C to the Golgi complex. When required, RAD51C is activated by the kinase ATM and recruited to the DNA damage site, where it engages other HR proteins to repair the incurred DNA lesions and, in turn, regulate DDR signalling. In line with the proposed model, we found that the redistribution of RAD51C by Giantin depletion impairs HR signalling response and results in a significant increase in genomic instability. Consistently, the knockdown of Giantin has been reported to inhibited HR repair rates[28] and phosphorylation of the DDR signalling protein, H2AX[29]. Nonetheless, we cannot exclude that the downregulation of Giantin impacts other nuclear events beyond the redistribution of RAD51C, although none of our data and previous literature would suggest this. Interestingly, similarly to Giantin, other members of the Golgin family have also been reported to HR rates [28] and DDR signalling protein[29]. Furthermore, numerous studies have also implicated the role of Giantin and the Golgins in cancer progression[14,35–37] and although further studies are required to clarify their role, these observations raise the intriguing possibility that this protein family can be integral for DDR regulation.

Taking in the wide array of the novel double-localising proteins identified in our study and their respective roles in important cellular processes such as membrane trafficking, and DDR, our results propose a high degree of interconnectivity between the Golgi and nuclear compartment. The Golgi complex has an established role in signalling, transport and post-translation modifications[1,38], our work here adds an additional so far unappreciated function, as part of DNA repair. Consistent with this thinking, we postulate that the Golgi, in its integrating function of several critical pathways, could act as a link to ensure that cellular homeostasis is maintained in response to DNA damage. It is tempting to speculate that the interaction we find for RAD51C and Giantin to regulate HR-mediated DNA repair could be extrapolated to the other DDR proteins identified from this study and their interaction with various other members of the Golgin protein family. Although, more work will be required to strengthen our hypothesis, our results and the large number of double-localising proteins identified in our study build a strong case in its support.

Taken together, our study presents strong evidence for a so far unappreciated Golgi regulatory pathway for the coordination of HR-mediated repair through the activity of RAD51C and Giantin. Furthermore, our results would also suggest that this regulation is not just restricted to HR-mediated DNA repair but could extend to all other types of DNA repair mechanisms such as NHEJ, MMR, and BER. This discovery has the potential to open new scientific fields from different ends and has the potential to significantly change the way we understand DNA repair regulation.

Materials and Methods

Antibodies and chemicals. Several commercially antibodies and chemical were used in the paper, including RAD51C (ab72063, Abcam; 1:500 for immunostaining) & (ab95069, Abcam, 1:2000 for western blotting; 1:500 for immunoprecipitation), GOLGB1/Giantin (AF8159, R&D systems; 1:500 for immunostaining and immunoprecipitation, 1:2000 for western blotting) & (G1/M1, Enzo Life Sciences, 1:500 for immunostaining), GM130 (610822, BD Biosciences, 1:500 for immunostaining, 1:2000 for western blotting), ATM Ser1981 (MA1-2020, Invitrogen; 1:500 for immunostaining; 1:2000 for western blotting), CHK2 pThr68 (PA5-17818, Invitrogen; 1:2000 for western blotting), DNA-PKcs (Ser2056) (PA5-78130, Invitrogen, 1:2000 for western blotting), gamma-H2AX pSer139 (613402, Biolegend; 1:500 for immunostaining, 1:2000 for western blotting), alpha-tubulin (MS-581, Thermo Fisher; 1:10,000 for western blotting) Lamin B1 (ab16048, Abcam; 1:2000 for western blotting) vinculin (ab219649, abcam; 1:2000 for western blotting), doxorubicin (ab120629, Abcam); Importazole (SML0341, Sigma-Aldrich), KU55933 (ATMi, SML1109, Sigma-Aldrich); ve-821 (ATRi, HY-14731; MedChemExpress) NU7441 (DNA-PKi, HY-11006; MedChemExpress), etoposide (ab120227, Abcam), mitomycin C (M7949, Sigma-Aldrich), and camptothecin (ab120115, Abcam).

Cell lines, cell culture and siRNA transfection. HeLa Kyoto, U2-O S, MCF7, were cultured in DMEM (Life Technologies) supplemented with 10% FBS (Invitrogen) and 1% L-glutamine (Invitrogen). Cells were checked for mycoplasma contamination by PCR. siRNA transfections were performed with Lipofectamine 2000 (Invitrogen) using SilencerSelect siRNAs (Ambion) according to the manufacturer's instructions. Transfections were carried out for 72 h and the final siRNA concentrations used were 15nM for all siRNAs. Giantin siRNA-1: 5951 & siRNA-2: 5953; GMAP210 siRNA-1: s17811 & siRNA-2: s17812; RAD51C siRNA: s11737.

Drug treatments. Cells were treated 24 h after seeding. For camptothecin, etoposide and mitomycin C experiments, cells were treated for 16 h at a concentration of 0.1 μM, 50μM and 5μM, respectively. After treatment cells were incubated with fresh medium for 2 hours. Doxorubicin was used at a concentration of 40μM for 3 h unless indicated otherwise. For kinase and importin-β inhibitor treatments, cells were pre-treated for 30 min with the described inhibitor prior to the addition of doxorubicin. The inhibitors were used at the following concentrations: importazole (IPZ) (20μM), KU55933 (ATMi) (30μM), NU7441 (DNA-Pki) (10μM) and ve-821 (ATRi) (10μM).

Immunofluorescence assay. Cells were fixed with 4% paraformaldehyde in PBS and permeabilized with 0.1% Triton X-100 for 15 min at room temperature, then cells were blocked with 5% bovine serum albumin in 0.05% Triton X-100 for 60 min and incubated with primary antibodies in blocking buffer at room temperature for 3 h. Following 3 washes with PBS, cells were incubated with fluorescent dye-conjugated secondary antibodies diluted in a blocking buffer for 1 h at room temperature.

Image and data analysis. Confocal microscopy experiments were performed with fixed and immunostained cell samples on a microscope FV3000, Olympus. Z stacks of images covering the entire cell thickness were acquired. All image analysis was performed using Cell Profiler[39] and Fiji[40]. Briefly, first nuclei were segmented in the Hoechst channel. When appropriate, the Golgi complex was segmented in the Golgi marker channel and using the segmented nuclei as seeds, the two structures were associated. Intensity profiles, morphology features and structuring counting analysis were performed when required using Cell Profiler.

Comet assay. The assay was carried out as previously described[41]. Briefly, cells were trypsinized, pelletized and resuspended in ice-cold PBS at a concentration of 25 × 10^4 cells per ml. The cells were resuspended in 2% low melting agarose (Sigma) and spread quickly onto gel bond film (Biozym) covered in 1% agarose (Sigma). Samples were immersed into a lysis buffer (100mM EDTA, 2.5M NaCl, 10mM Tris-HCl and 1% Triton-X100; pH 10) overnight at 4°C. Followed by a wash with ice cold water and run in an electrophoresis chamber (alkaline buffer: 1mM EDTA, 300mM NaOH; pH 13) at 15V, 300mA for 60 min at 4°C. Slides were first washed in a Tris-HCl neutralisation buffer (0.4M; pH 7.5) followed by water, stained with SYBR Gold (Thermo Fisher Scientific) (1:10000) and finally dried. Comets were imaged by automated Olympus Scan^R screening microscope and comet tails scored using OpenComet plugin (Gyori et al., 2014).

Western blotting analysis. HK cells were lysed using RIPA buffer (Thermo Scientific) with complete protease inhibitor cocktail (Roche). SDS-PAGE was performed on pre-cast Tris-Acetate gels followed by transfer to PVDF transfer membrane (Merck Millipore). Proteins were detected using primary antibodies as described followed by incubation with secondary antibodies coupled with HRP (Invitrogen). Detection of protein was performed using Pierce ECL Plus Western Blotting Substrate reagent (Thermo Scientific) and visualised on Azure 280 chemiluminescent imaging system. Subcellular fractionation was performed using a subcellular protein fractionation kit for cultured cells (Thermo scientific) according to the manufacturer's instructions. Fractions were verified using well-established markers (GM130 for Golgi membranes, Lamin B1 for the nuclear compartment, alpha-tubulin for the cytoplasmic fraction) and probed for RAD51C presence in each compartment. The RAD51C membrane:nuclear distribution ratio was calculated by first dividing the RAD51C protein level in each fraction by the protein level of the appropriate control, the resulting membrane (M_{R51C} / M_{GM130}) and nuclear (N_{R51C} / $N_{laminB1}$) ratios were further divided to give the ratio = (M_{R51C} / M_{GM130}) / (N_{R51C} / $N_{laminB1}$). The ratios obtained from the control were normalised to 1 and compared to the treated group.

Immunoprecipitation. HK cells were lysed using a lysis buffer (50mM Hepes, 130mM NaCl, 1mM DTT 1% NP-40) with complete protease inhibitor cocktail (Roche). Cell lysates were centrifuged at 13,000 rpm for 10 mins at 4°C. For immunoprecipitation, the lysates were incubated with the primary antibody described and rotated overnight at 4°C. Next, the lysates were incubated with G-agarose beads (Roche) and rotated for 4 h at 4°C. The samples were washed with cold lysis buffer and then precipitated proteins were eluted by 2x SDS sample buffer and analysed by Western blotting.

Localisation validation siRNA assay. A custom-designed siRNA library targeting our proteins of interest (Ambion) was designed and prepared in 96-well glass bottom plates (Miltenyi Biotec) using a protocol for solid phase reverse transfection as previously described[16,42]. Non-targeting siRNA was used as a negative control. 72 hours after cell seeding, cells were fixed with 4% paraformaldehyde, permeabilized with 0.1% Triton-X100 and immunostained against the HPA antibodies of interest and a Golgi marker, GM130. Hoechst 33342 was used as a nuclear stain. siRNAs and antibodies details are available in **Supplementary table S1**. Images were acquired on a fully automated Molecular Devices IXM with a 10x/0.45 NA P-APO objective. The resulting images were analysed using Cell Profiler software [39] for quantitative and automated measurements of fluorescence from the antibodies

as previously described[16]. Briefly, nuclei were segmented in the Hoechst channel, the Golgi complex was segmented in the Golgi marker channel and using the segmented nuclei as seeds, the two structures were associated. Intensity profiles of each compartment were acquired. Reduction of 25% or more of the antibody staining in both Golgi and nuclear compartments was considered as a validation of the antibody specificity (**Supplementary table S1**).

Statistical analysis. All data were obtained from at least three independent experiments if not otherwise stated. Statistical analyses were performed using two tailed t-test for pairwise comparison and one-way analysis of variance (ANOVA) for multiple comparisons on GraphPad Prism 9. Data are expressed as standard error of the mean (s.e.m.). n values indicate biologically independent samples and experiments. $P < 0.05$ was considered statistically significant.

Acknowledgements. We thank the ALMF, FCCF and the Pepperkok team for their support. In addition, we acknowledge Jan Ellenberg, Claudia Lukas, Diana Ordonez and Simone Köhler for their assistance in developing the project and manuscript. G.G. was supported by the EMBL EIPOD programme, K.K. by the EMBL PhD programme and M.M.K. by the German Centre for Lung Research.

Figure legend

Figure 1.* RAD51C localises to both the Golgi and nuclear compartment and *redistributes in response to DNA damage events. (a) STRING protein-protein interaction network showing the DDR proteins identified to localise to both the Golgi complex and nucleus; yellow nodes indicate double-localising proteins, grey nodes are filler untested proteins; experimentally-based string network. (b) Representative images of HeLa Kyoto cells stained with antibodies against RAD51C (green) and GM130 (red). DNA was stained with Hoechst 33342 (blue). (c) Western blot showing the subcellular membrane (M), nuclear (N) and cytoplasmic (C) fractions of RAD51C markers (GM130 for Golgi membranes, Lamin B1 for the nuclear compartment, alpha-tubulin for the cytoplasmic fraction) ($n = 3$ biologically independent experiments). (d) HK cells treated with the DNA damage inducing drug, doxorubicin (DOX), for increasing lengths of time. Yellow arrows denote the Golgi membrane; white arrows denote nuclear foci; scale bar: 10 μm. (e) Quantification of sum intensity of RAD51C Golgi population, (f) RAD51C nuclear population, and (g) a ratio of RAD51C Golgi-nuclear distribution after treatment with DOX. Data represent the mean ± standard error of the mean (s.e.m.) ($n = 3$ biologically independent samples with a total of 2343 cells analysed). P values were determined by one-way analysis of variance (ANOVA).

Figure 2. Redistribution of RAD51C Golgi fraction is required for the formation of RAD51C nuclear foci and is dependent on the kinase ATM. HK cells were stained with antibodies against RAD51C and GM130. (a) Cells were treated with DMSO or IPZ prior to a 3-hour treatment with DOX. Yellow arrows denote the Golgi membrane; white denote nuclear foci. Results were quantified as (b) relative sum intensity of RAD51C at the Golgi and (c) ratio of RAD51C Golgi-nuclear distribution. Scale bar 10 μm. Data represent the mean ± standard error of the mean (s.e.m.) ($n = 3$ biologically independent samples with a total of 445 cells analysed). (d) HK cells were treated with DMSO (control) alone or with ATM inhibitor (KU55933) or ATR inhibitor (VE-821) or DNA-PK inhibitor (NU7441) prior to a 3-hour treatment

with doxorubicin. Results were quantified as an (e) relative sum intensity of RAD51C at the Golgi and (f) ratio of RAD51C Golgi-nuclear distribution. Scale bar 10 μm. Data represent the mean ± standard error of the mean (s.e.m.) ($n = 3$ biologically independent samples with a total of 1679 cells analysed). Statistical significance was determined using one-way analysis of variance (ANOVA).

Figure 3. RAD51C Golgi localization and activation is dependent on the Golgin protein Giantin. (a) HK cells were transfected with control, or Giantin siRNAs for 72 hours. The cells were stained with antibodies against RAD51C and Golgi marker, GM130. Yellow arrows indicate the Golgi and white arrows indicate nuclear foci; scale bar 10 μm. Quantification of the localisation changes of RAD51C were quantified as (b) relative sum intensity of RAD51C at the Golgi, (c) fluorescent intensity ratio of the RAD51C Golgi-nuclear distribution and (d) relative number of RAD51C foci per cell. Data represent the mean ± standard error of the mean (s.e.m.) ($n = 3$ biologically independent samples with a total of 1445 cell analysed). Statistical significance was determined using one-way ANOVA; (e) Immunoprecipitation of Giantin with RAD51C.

Figure 4. Colocalization analysis of RAD51C nuclear foci induced by Giantin depletion with DDR markers. (a-d) Co-localisation experiment of cells treated with control siRNA, or Giantin siRNA. Cell stain with antibody against RAD51C (green) and HR DDR markers (red): (a) y-H2AX, and (c) p-ATM. Co-localisation of structure is denoted by an arrow; Scale bar 10 μm. Quantification of percentage RAD51C foci co-localising with (b) y-H2AX and (d) p-ATM. Data represent the mean ± standard error of the mean (s.e.m.) ($n = 3$ biologically independent samples with a total number of 318 and 285 cells analysed for the colocalization experiments with y-H2AX and p-ATM, respectively). Statistical significance was determined using a two-tailed unpaired Student's *t*-test.

Figure 5. Depletion of Giantin led to increased genomic instability and disruption of DDR signalling. (a) Representative images of comet assay detection genomic DNA fragmentation in HK cells treated with control, Giantin, or RAD51C targeting siRNA. (b) Quantification of comet OliveMoment. Data represent the mean ± standard error of the mean (s.e.m.). ($n = 3$ biologically independent samples with 1552 cells analysed). Statistical significance was determined using one-way analysis of variance (ANOVA); (c, d) Representative images and quantification of percentage cells displaying micronuclei after siRNA treatment; scale bar 10 μm. White arrows denote micronuclei structures. Data represent the mean ± standard error of the mean (s.e.m.) ($n = 3$ biologically independent samples with over 10,000 cell analysed). Statistical significance was determined using one-way analysis of variance (ANOVA). (e, f) HK cells transfected with control or Giantin siRNAs and treated with doxorubicin or camptothecin after 72 h transfection, the extracts were prepared and immunoblotted as indicated ($n = 2$ biologically independent samples). (g) Cell cycle profile of HK cell treated with Giantin or control siRNA. Data represent the mean ± standard error of the mean (s.e.m.) ($n = 3$ biologically independent samples).

Figure 6. **Proposed model for the regulation of HR-mediated repair through the activation of RAD51C at the Golgi complex.** RAD51C, a regulatory HR protein, is anchored to the Golgi through its interaction with cytoplasmic tail of Giantin, in response to double-strand DNA breaks, this RAD51C Golgi population redistributes to form nuclear foci. This response

requires importin-beta mediated nuclear import and the phosphorylation of ATM protein kinase.

EXTENDED DATA FIGURE 1. (a) Representative images showing U-2 OS and MCF7 cells stained with antibodies against RAD51C (green) and GM130 (red). DNA was stained with Hoechst 33342 (blue). (b) Representative images showing the RAD51C antibody specificity. HK cells are stained with antibodies against RAD51C and GM130; DNA was stained with Hoechst 33342. (c) Quantification of RAD51C sum intensity after RAD51C depletion. Data represent the mean ± standard error of the mean (s.e.m.). ($n = 3$ biologically independent samples with a total of 831 cells analysed). (d) Western blot showing the level of RAD51C protein level, in RAD51C-depleted and control cells ($n = 3$ biologically independent samples). (e) Western blot showing the subcellular localization of RAD51C treated with the DMSO and doxorubicin. (f) Quantification of WB showing a ratio of RAD51C membrane-nuclear distribution. Data represent the mean ± standard error of the mean (s.e.m.) ($n = 2$ biologically independent samples). Statistical significance was determined using a two-tailed unpaired Student's *t*-test.

EXTENDED DATA FIGURE 2. Representative images of HK cells were stained with antibodies against RAD51C and GM130. HK cells were treated with DMSO (control) alone or with ATM inhibitor (KU55933) or ATR inhibitor (VE-821) or DNA-PK inhibitor (NU7441); scale bar 10 µm.

EXTENDED DATA FIGURE 3. HK cell stained with antibodies against RAD51C and GM130. Cells were treated with (a) Camptothecin (CPT), (d) etoposide (ETO) and (g) mitomycin C (MMC) for 16 h followed by media change for 2 h; scale bar 10 µm. Quantification of RAD51C percentage distribution between the Golgi and nuclear compartment after (b) CPT, (e) ETO and (h) MMC treatments. Quantification of RAD51C percentage distribution between the Golgi and nuclear compartment after (c) CPT, (f) ETO and (i) MMC treatments. treatments. Data represent the mean ± standard error of the mean (s.e.m.). ($n = 3$ biologically independent samples with more than 600 cells analysed per treatment). Statistical significance was determined using a two-tailed unpaired Student's *t*-test.

EXTENDED DATA FIGURE 4. (a) siRNA screen data (Adamson *et al*, 2012) showing the relative homologous recombination (HR) repair rate upon systematic knockdown of the Golgin protein family (grey) and HR complex proteins (black). (b) siRNA screen data (Paulsen et al., 2009) showing the relative percent cell population with phosphorylation of H2AX upon systematic knockdown of the Golgins. The datasets are normalised to the negative control set at 1. (c) HK cells were transfected with control, or Giantin siRNAs for 72 hours. The cells were stained with antibodies against Giantin and nuclei stained with Hoechst 33342; scale bar 10 µm.

References

1. Wilson, C. *et al.* The Golgi apparatus: an organelle with multiple complex functions. *Biochem. J* **433**, 1–9 (2011).
2. Makhoul, C., Gosavi, P. & Gleeson, P. A. The Golgi architecture and cell sensing. *Biochem. Soc. Trans.* **46**, 1063–1072 (2018).
3. Machamer, C. E. The Golgi complex in stress and death. *Front. Neurosci.* **9**, (2015).

4. Liu, J. *et al.* The role of the Golgi apparatus in disease. *Int. J. Mol. Med.* **47**, (2021).
5. Zappa, F., Failli, M. & De Matteis, M. A. The Golgi complex in disease and therapy. *Curr. Opin. Cell Biol.* **50**, 102–116 (2018).
6. Freeze, H. H. & Ng, B. G. Golgi Glycosylation and Human Inherited Diseases. *Cold Spring Harb. Perspect. Biol.* **3**, 1–22 (2011).
7. Brown, M. S., Radhakrishnan, A. & Goldstein, J. L. Retrospective on Cholesterol Homeostasis: The Central Role of Scap. *Annu. Rev. Biochem.* **87**, 783–807 (2018).
8. Haze, K., Yoshida, H., Yanagi, H., Yura, T. & Mori, K. Mammalian transcription factor ATF6 is synthesized as a transmembrane protein and activated by proteolysis in response to endoplasmic reticulum stress. *Mol. Biol. Cell* **10**, 3787–3799 (1999).
9. Colanzi, A. & Sütterlin, C. Signaling at the Golgi during mitosis. *Methods Cell Biol.* **118**, 383–400 (2013).
10. Kulkarni-Gosavi, P., Makhoul, C. & Gleeson, P. A. Form and function of the Golgi apparatus: scaffolds, cytoskeleton and signalling. *FEBS Lett.* **593**, 2289–2305 (2019).
11. Petrosyan, A. Onco-Golgi: Is Fragmentation a Gate to Cancer Progression? *Biochem. Mol. Biol. J.* **01**, 1–11 (2015).
12. Zhang, X. Alterations of Golgi Structural Proteins and Glycosylation Defects in Cancer. *Front Cell Dev Biol* **9**, 665289 (2021).
13. Farber-Katz, S. E. *et al.* DNA damage triggers golgi dispersal via DNA-PK and GOLPH3. *Cell* **156**, 413–427 (2014).
14. Bui, S., Mejia, I., Diaz, B. & Wang, Y. Adaptation of the Golgi Apparatus in Cancer Cell Invasion and Metastasis. *Front Cell Dev Biol* **9**, 806482 (2021).
15. Thul, P. J. *et al.* A subcellular map of the human proteome. *Science (80-.).* **356**, (2017).
16. Stadler, C. *et al.* Systematic validation of antibody binding and protein subcellular localization using siRNA and confocal microscopy. *J. Proteomics* **75**, 2236–2251 (2012).
17. Prakash, R., Zhang, Y., Feng, W. & Jasin, M. Homologous recombination and human health: the roles of BRCA1, BRCA2, and associated proteins. *Cold Spring Harb. Perspect. Biol.* **7**, a016600 (2015).
18. Rein, H. L., Bernstein, K. A. & Baldock, R. A. RAD51 paralog function in replicative DNA damage and tolerance. *Curr. Opin. Genet. Dev.* **71**, 86–91 (2021).
19. Sullivan, M. R. & Bernstein, K. A. RAD-ical new insights into RAD51 regulation. *Genes (Basel).* **9**, (2018).
20. Badie, S. *et al.* RAD51C facilitates checkpoint signaling by promoting CHK2 phosphorylation. *J. Cell Biol.* **185**, 587–600 (2009).
21. Thorn, C. F. *et al.* Doxorubicin pathways: pharmacodynamics and adverse effects. *Pharmacogenet. Genomics* **21**, 440 (2011).
22. Soderholm, J. F. *et al.* Importazole, a small molecule inhibitor of the transport receptor importin-β. *ACS Chem. Biol.* **6**, 700–708 (2011).
23. Ciccia, A. & Elledge, S. J. The DNA Damage Response: Making It Safe to Play with Knives. *Mol. Cell* **40**, 179–204 (2010).
24. Hickson, I. *et al.* Identification and characterization of a novel and specific inhibitor of the ataxia-telangiectasia mutated kinase ATM. *Cancer Res.* **64**, 9152–9159 (2004).
25. Fokas, E. *et al.* Targeting ATR in vivo using the novel inhibitor VE-822 results in selective sensitization of pancreatic tumors to radiation. *Cell Death \& Disease* vol. 3 e441--e441 (2012).
26. Tavecchio, M., Munck, J. M., Cano, C., Newell, D. R. & Curtin, N. J. Further characterisation of the cellular activity of the DNA-PK inhibitor, NU7441, reveals potential cross-talk with homologous recombination. *Cancer Chemother. Pharmacol.* **69**, 155–164 (2012).
27. Jekimovs, C. *et al.* Chemotherapeutic compounds targeting the DNA double-strand break repair pathways: the good, the bad, and the promising. *Front. Oncol.* **4**, 86 (2014).
28. Adamson, B., Smogorzewska, A., Sigoillot, F. D., King, R. W. & Elledge, S. J. A genome-wide homologous recombination screen identifies the RNA-binding protein RBMX as a component of the DNA-damage response. *Nat. Cell Biol.* **14**, 318–328

(2012).
29. Paulsen, R. D. *et al.* A genome-wide siRNA screen reveals diverse cellular processes and pathways that mediate genome stability. *Mol. Cell* **35**, 228–239 (2009).
30. Witkos, T. M. & Lowe, M. The Golgin Family of Coiled-Coil Tethering Proteins. *Front Cell Dev Biol* **3**, 86 (2015).
31. Vitor, A. C., Huertas, P., Legube, G. & de Almeida, S. F. Studying DNA Double-Strand Break Repair: An Ever-Growing Toolbox. *Front Mol Biosci* **7**, 24 (2020).
32. Møller, P. The comet assay: ready for 30 more years. *Mutagenesis* **33**, 1–7 (2018).
33. Olive, P. L., Banáth, J. P. & Durand, R. E. Heterogeneity in Radiation-Induced DNA Damage and Repair in Tumor and Normal Cells Measured Using the Comet Assay. *Radiation Research* vol. 178 AV35--AV42 (2012).
34. Brandsma, I. & Gent, D. C. Pathway choice in DNA double strand break repair: observations of a balancing act. *Genome Integr.* **3**, 9 (2012).
35. Baschieri, F., Uetz-von Allmen, E., Legler, D. F. & Farhan, H. Loss of GM130 in breast cancer cells and its effects on cell migration, invasion and polarity. *Cell Cycle* **14**, 1139–1147 (2015).
36. Bhat, G., Hothpet, V. R., Lin, M. F. & Cheng, P. W. Shifted Golgi targeting of glycosyltransferases and α-mannosidase IA from giantin to GM130-GRASP65 results in formation of high mannose N-glycans in aggressive prostate cancer cells. *Biochim. Biophys. Acta - Gen. Subj.* **1861**, 2891–2901 (2017).
37. Ghannoum, S. *et al. A combined experimental-computational approach uncovers a role for the Golgi matrix protein Giantin in breast cancer progression*. *bioRxiv* (2022).
38. Jackson, C. L. Mechanisms of transport through the Golgi complex. *J. Cell Sci.* **122**, 443–452 (2009).
39. Carpenter, A. E. *et al.* CellProfiler: image analysis software for identifying and quantifying cell phenotypes. *Genome Biol.* **7**, R100 (2006).
40. Schindelin, J. *et al.* Fiji: an open-source platform for biological-image analysis. *Nat. Methods* **9**, 676–682 (2012).
41. Vodenkova, S. *et al.* An optimized comet-based in vitro DNA repair assay to assess base and nucleotide excision repair activity. *Nat. Protoc.* **15**, 3844–3878 (2020).
42. Erfle, H. *et al.* Work flow for multiplexing siRNA assays by solid-phase reverse transfection in multiwell plates. *J. Biomol. Screen.* **13**, 575–580 (2008).

FIGURE 1

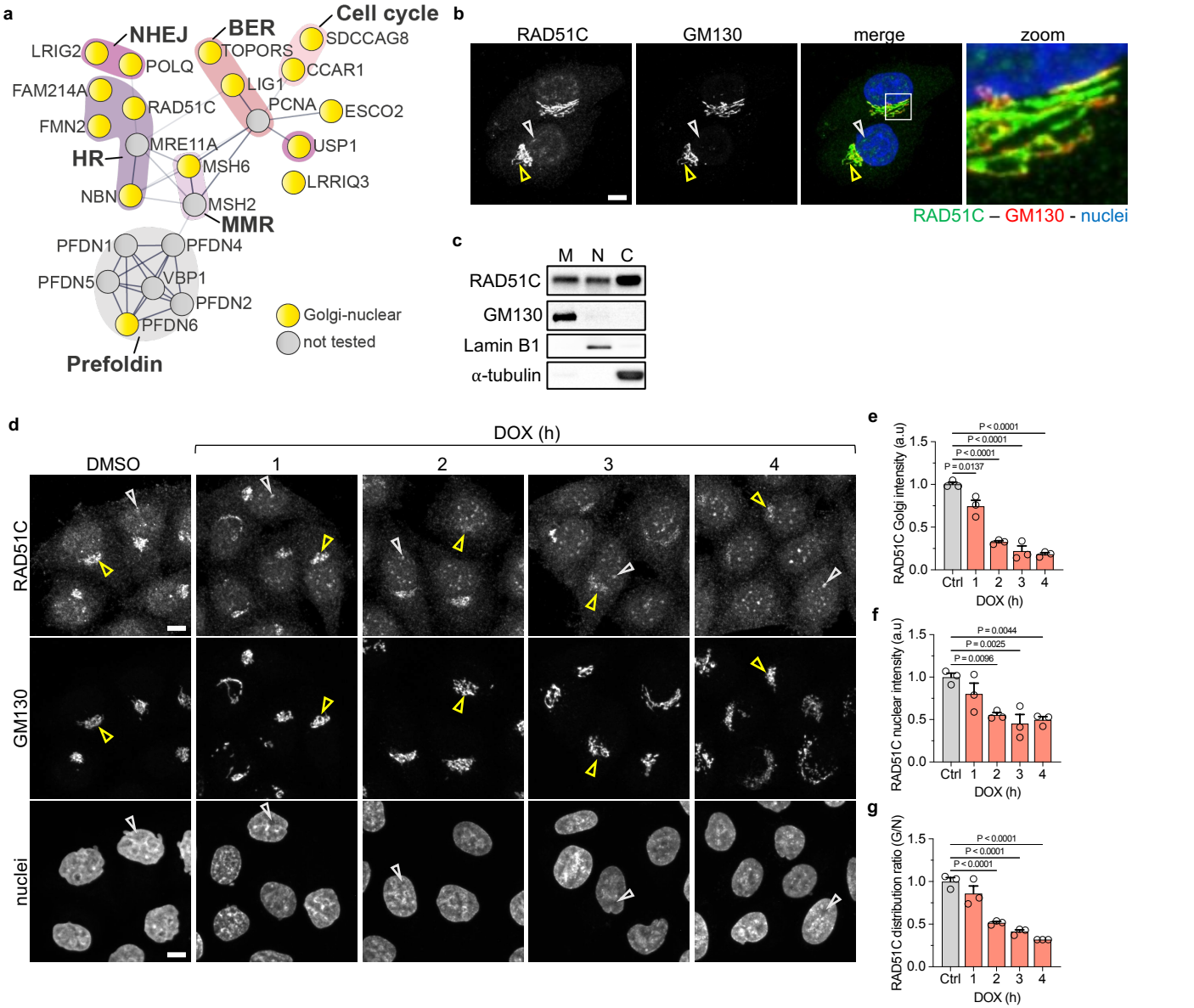

Figure 1. RAD51C localises to both the Golgi and nuclear compartment and redistributes in response to DNA damage events. (a) STRING protein-protein interaction network showing the DDR proteins identified to localise to both the Golgi complex and nucleus; yellow nodes indicate double-localising proteins, grey nodes are filler untested proteins; experimentally-based string network. (b) Representative images of HeLa Kyoto cells stained with antibodies against RAD51C (green) and GM130 (red). DNA was stained with Hoechst 33342 (blue). (c) Western blot showing the subcellular membrane (M), nuclear (N) and cytoplasmic (C) fractions of RAD51C markers (GM130 for Golgi membranes, Lamin B1 for the nuclear compartment, alpha-tubulin for the cytoplasmic fraction) (n = 3 biologically independent experiments). (d) HK cells treated with the DNA damage inducing drug, doxorubicin (DOX), for increasing lengths of time. Yellow arrows denote the Golgi membrane; white arrows denote nuclear foci; scale bar: 10 μm. (e) Quantification of sum intensity of RAD51C Golgi population, (f) RAD51C nuclear population, and (g) a ratio of RAD51C Golgi-nuclear distribution after treatment with DOX. Data represent the mean ± standard error of the mean (s.e.m.) (n = 3 biologically independent samples with a total of 2343 cells analysed). P values were determined by one-way analysis of variance (ANOVA).

FIGURE 2

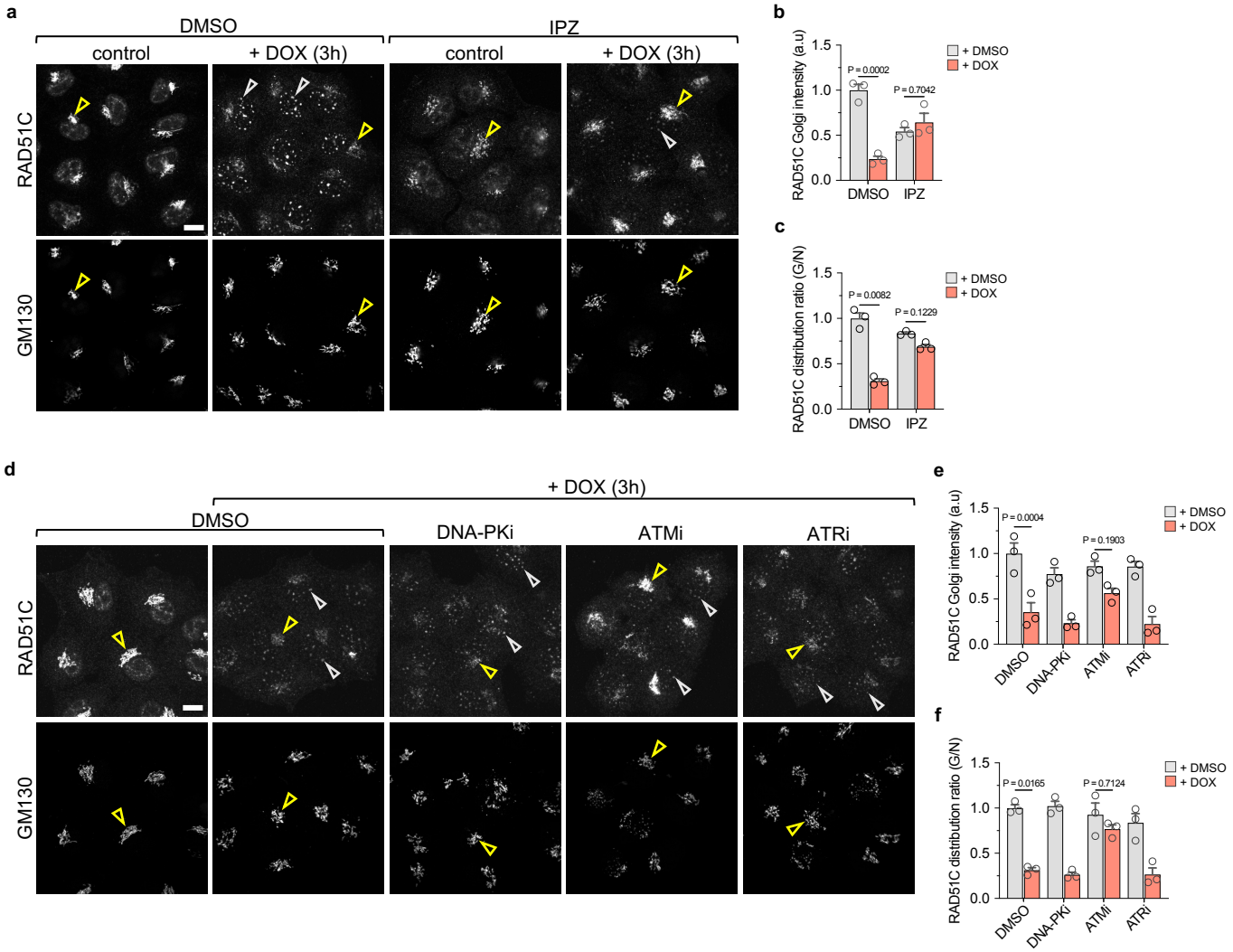

Figure 2. Redistribution of RAD51C Golgi fraction is required for the formation of RAD51C nuclear foci and is dependent on the kinase ATM. HK cells were stained with antibodies against RAD51C and GM130. (a) Cells were treated with DMSO or IPZ prior to a 3-hour treatment with DOX. Yellow arrows denote the Golgi membrane; white denote nuclear foci. Results were quantified as (b) relative sum intensity of RAD51C at the Golgi and (c) ratio of RAD51C Golgi-nuclear distribution. Scale bar 10 μm. Data represent the mean ± standard error of the mean (s.e.m.) (n = 3 biologically independent samples with a total of 445 cells analysed). (d) HK cells were treated with DMSO (control) alone or with ATM inhibitor (KU55933) or ATR inhibitor (VE-821) or DNA-PK inhibitor (NU7441) prior to a 3-hour treatment with doxorubicin. Results were quantified as an (e) relative sum intensity of RAD51C at the Golgi and (f) ratio of RAD51C Golgi-nuclear distribution. Scale bar 10 μm. Data represent the mean ± standard error of the mean (s.e.m.) (n = 3 biologically independent samples with a total of 1679 cells analysed). Statistical significance was determined using one-way analysis of variance (ANOVA).

FIGURE 3

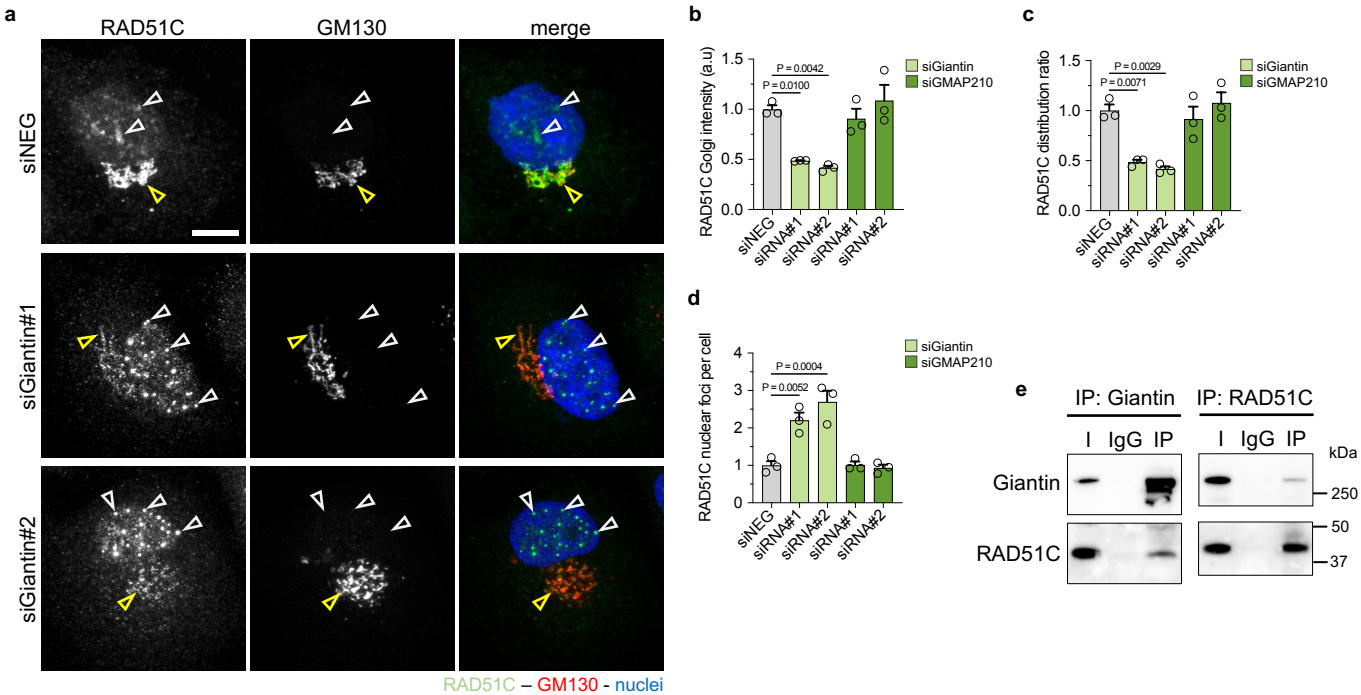

Figure 3. RAD51C Golgi localization and activation is dependent on the Golgin protein Giantin. (a) HK cells were transfected with control, or Giantin siRNAs for 72 hours. The cells were stained with antibodies against RAD51C and Golgi marker, GM130. Yellow arrows indicate the Golgi and white arrows indicate nuclear foci; scale bar 10 μm. Quantification of the localisation changes of RAD51C were quantified as (b) relative sum intensity of RAD51C at the Golgi, (c) fluorescent intensity ratio of the RAD51C Golgi-nuclear distribution and (d) relative number of RAD51C foci per cell. Data represent the mean ± standard error of the mean (s.e.m.) (n = 3 biologically independent samples with a total of 1445 cell analysed). Statistical significance was determined using one-way ANOVA; (e) Immunoprecipitation of Giantin with RAD51C.

FIGURE 4

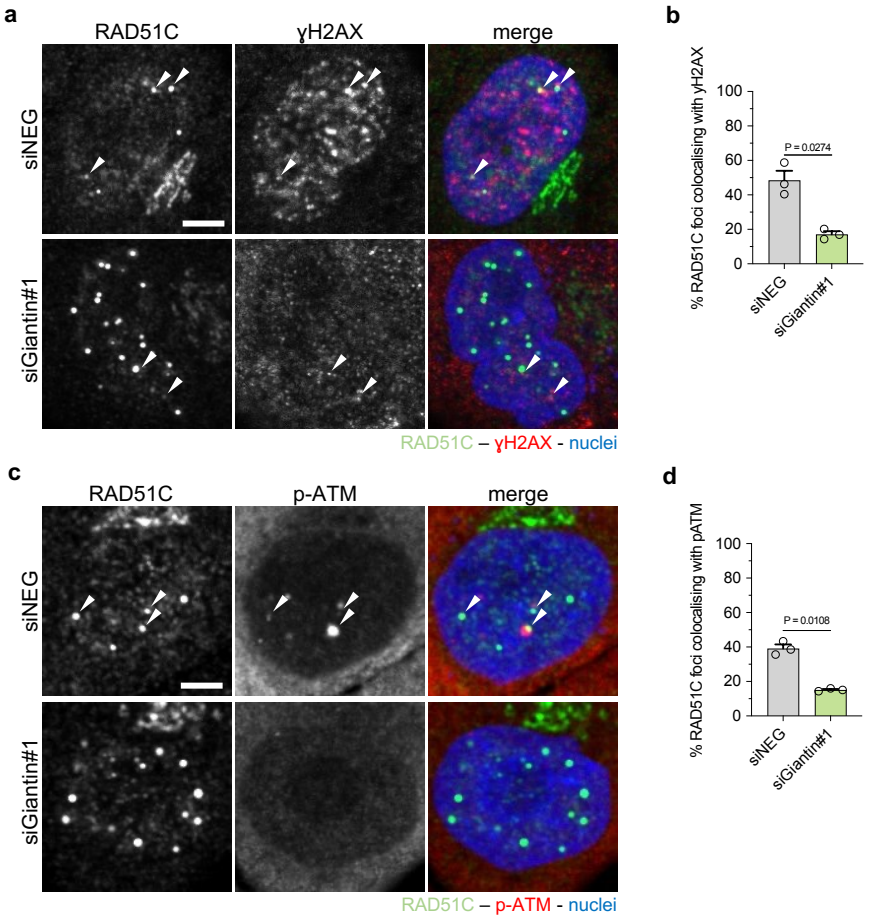

Figure 4. Colocalization analysis of RAD51C nuclear foci induced by Giantin depletion with DDR markers. (a-d) Co-localisation experiment of cells treated with control siRNA, or Giantin siRNA. Cell stain with antibody against RAD51C (green) and HR DDR markers (red): (a) y-H2AX, and (c) p-ATM. Co-localisation of structure is denoted by an arrow; Scale bar 10 μm. Quantification of percentage RAD51C foci co-localising with (b) y-H2AX and (d) p-ATM. Data represent the mean ± standard error of the mean (s.e.m.) (n = 3 biologically independent samples with a total number of 318 and 285 cells analysed for the colocalization experiments with y-H2AX and p-ATM, respectively). Statistical significance was determined using a two-tailed unpaired Student's t-test.

FIGURE 5

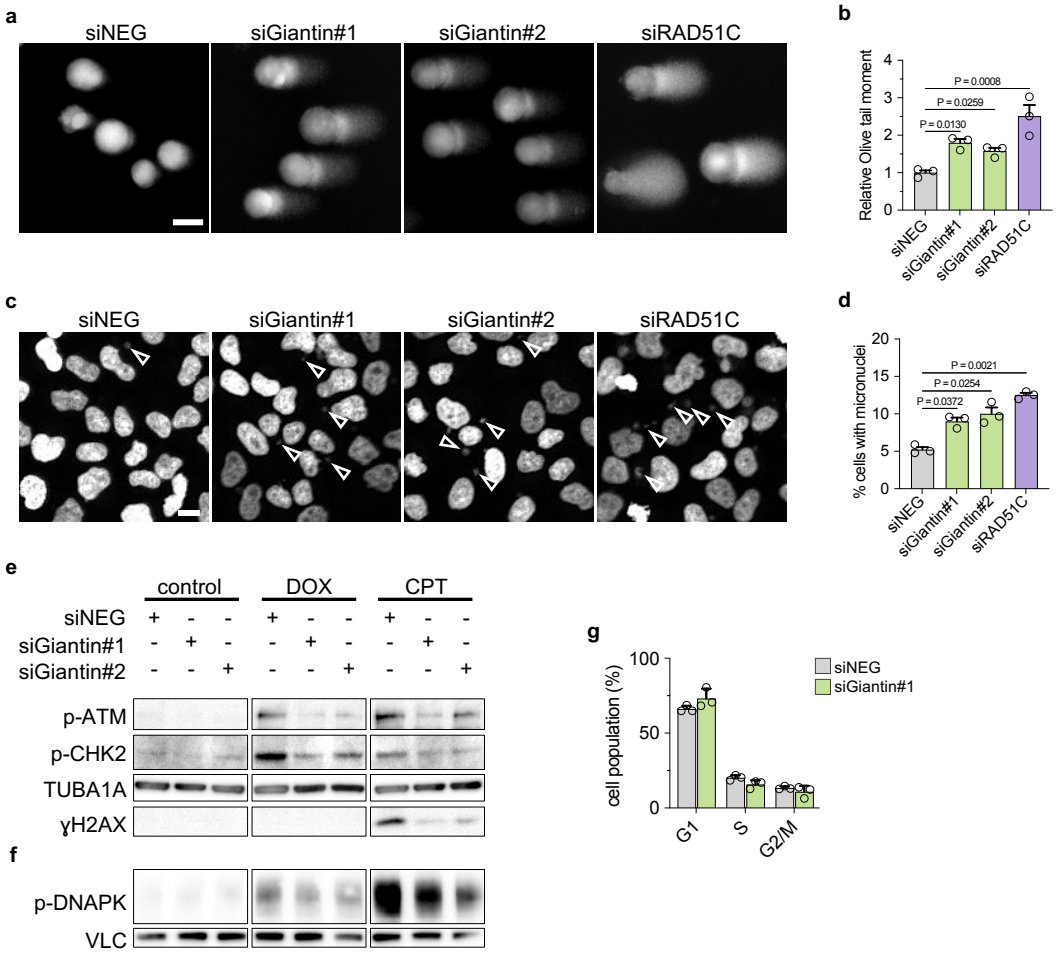

Figure 5. Depletion of Giantin led to increased genomic instability and disruption of DDR signalling. (a) Representative images of comet assay detection genomic DNA fragmentation in HK cells treated with control, Giantin, or RAD51C targeting siRNA. (b) Quantification of comet OliveMoment. Data represent the mean ± standard error of the mean (s.e.m.). (n = 3 biologically independent samples with 1552 cells analysed). Statistical significance was determined using one-way analysis of variance (ANOVA); (c, d) Representative images and quantification of percentage cells displaying micronuclei after siRNA treatment; scale bar 10 μm. White arrows denote micronuclei structures. Data represent the mean ± standard error of the mean (s.e.m.) (n = 3 biologically independent samples with over 10,000 cell analysed). Statistical significance was determined using one-way analysis of variance (ANOVA). (e, f) HK cells transfected with control or Giantin siRNAs and treated with doxorubicin or camptothecin after 72 h transfection, the extracts were prepared and immunoblotted as indicated (n = 2 biologically independent samples). (g) Cell cycle profile of HK cell treated with Giantin or control siRNA. Data represent the mean ± standard error of the mean (s.e.m.) (n = 3 biologically independent samples).

FIGURE 6

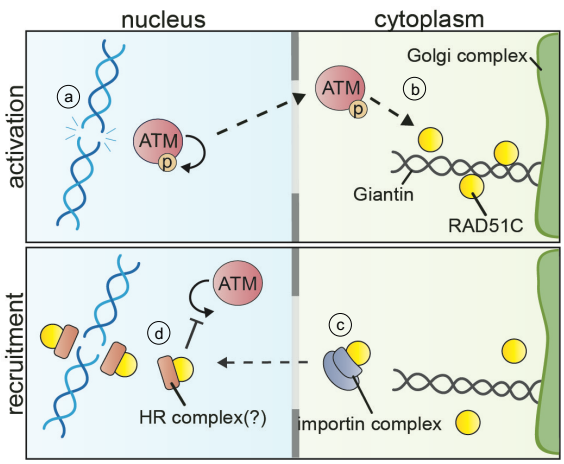

Figure 6. Proposed model for the regulation of HR-mediated repair through the activation of RAD51C at the Golgi complex. RAD51C, a regulatory HR protein, is anchored to the Golgi through its interaction with cytoplasmic tail of Giantin, in response to double-strand DNA breaks, this RAD51C Golgi population redistributes to form nuclear foci. This response requires importin-beta mediated nuclear import and the phosphorylation of ATM protein kinase.

EXTENDED DATA FIGURE 1

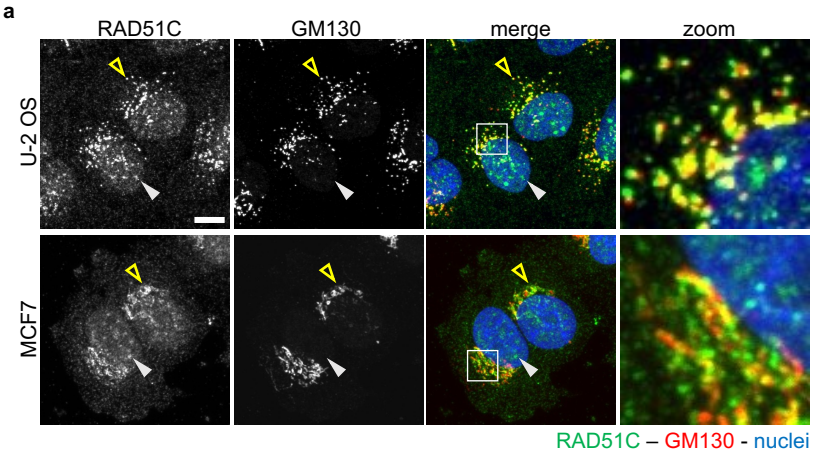

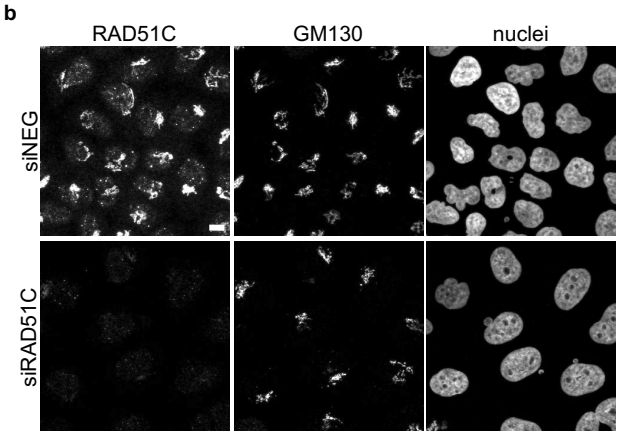

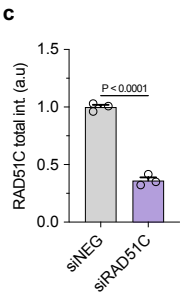

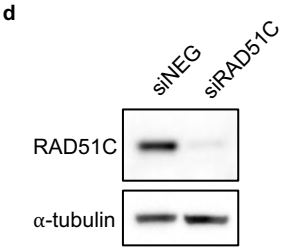

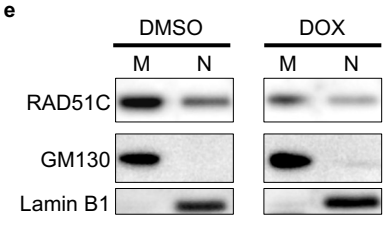

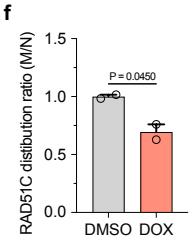

EXTENDED DATA FIGURE 1. (a) Representative images showing U-2 OS and MCF7 cells stained with antibodies against RAD51C (green) and GM130 (red). DNA was stained with Hoechst 33342 (blue). (b) Representative images showing the RAD51C antibody specificity. HK cells are stained with antibodies against RAD51C and GM130; DNA was stained with Hoechst 33342. (c) Quantification of RAD51C sum intensity after RAD51C depletion. Data represent the mean ± standard error of the mean (s.e.m.). (n = 3 biologically independent samples with a total of 831 cells analysed). (d) Western blot showing the level of RAD51C protein level, in RAD51C-depleted and control cells (n = 3 biologically independent samples). (e) Western blot showing the subcellular localization of RAD51C treated with the DMSO and doxorubicin. (f) Quantification of WB showing a ratio of RAD51C membrane-nuclear distribution. Data represent the mean ± standard error of the mean (s.e.m.) (n = 2 biologically independent samples). Statistical significance was determined using a two-tailed unpaired Student's t-test.

EXTENDED DATA FIGURE 2

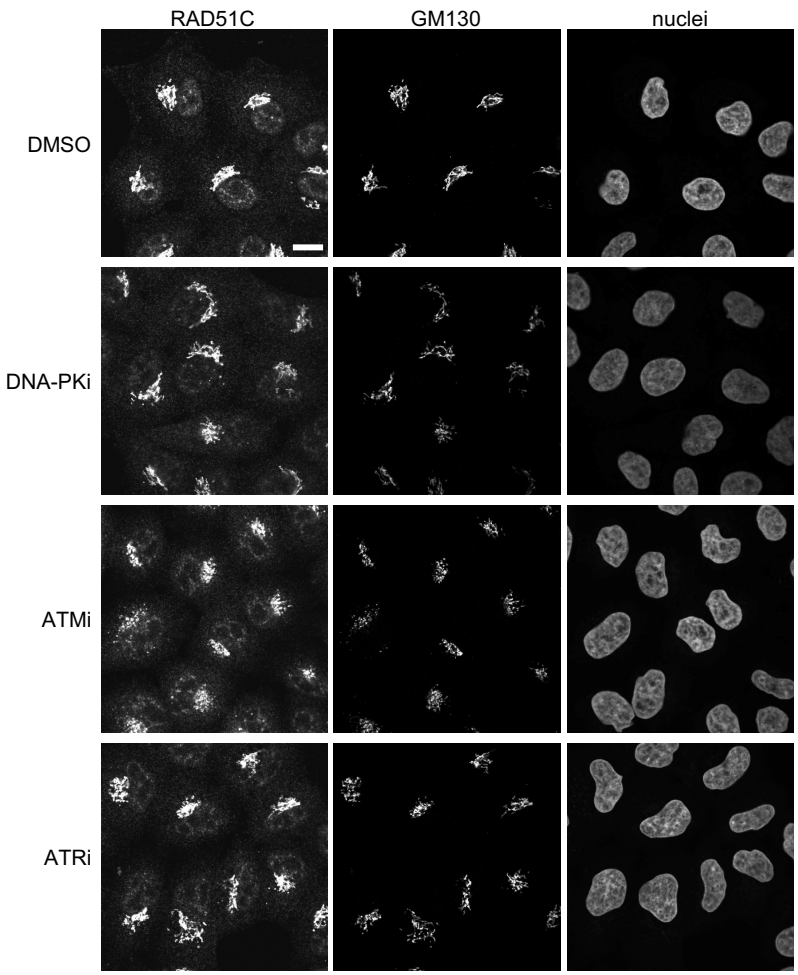

EXTENDED DATA FIGURE 2. Representative images of HK cells were stained with antibodies against RAD51C and GM130. HK cells were treated with DMSO (control) alone or with ATM inhibitor (KU55933) or ATR inhibitor (VE-821) or DNA-PK inhibitor (NU7441); scale bar 10 μm.

EXTENDED DATA FIGURE 3

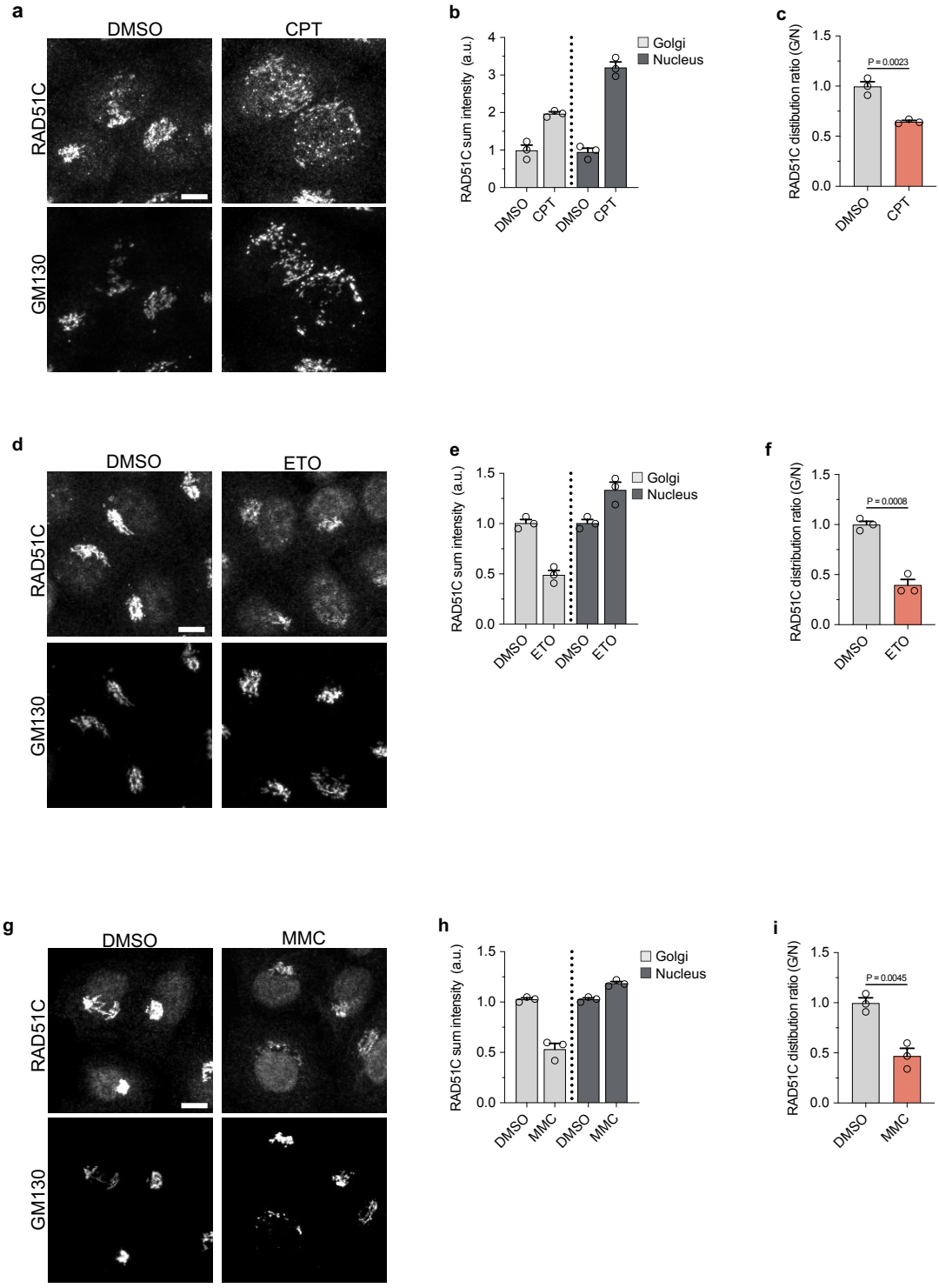

EXTENDED DATA FIGURE 3. HK cell stained with antibodies against RAD51C and GM130. Cells were treated with (a) Camptothecin (CPT), (d) etoposide (ETO) and (g) mitomycin C (MMC) for 16 h followed by media change for 2 h; scale bar 10 µm. Quantification of RAD51C percentage distribution between the Golgi and nuclear compartment after (b) CPT, (e) ETO and (h) MMC treatments. Quantification of RAD51C percentage distribution between the Golgi and nuclear compartment after (c) CPT, (f) ETO and (i) MMC treatments. treatments. Data represent the mean ± standard error of the mean (s.e.m.). (n = 3 biologically independent samples with more than 600 cells analysed per treatment). Statistical significance was determined using a two-tailed unpaired Student's t-test.

EXTENDED DATA FIGURE 4

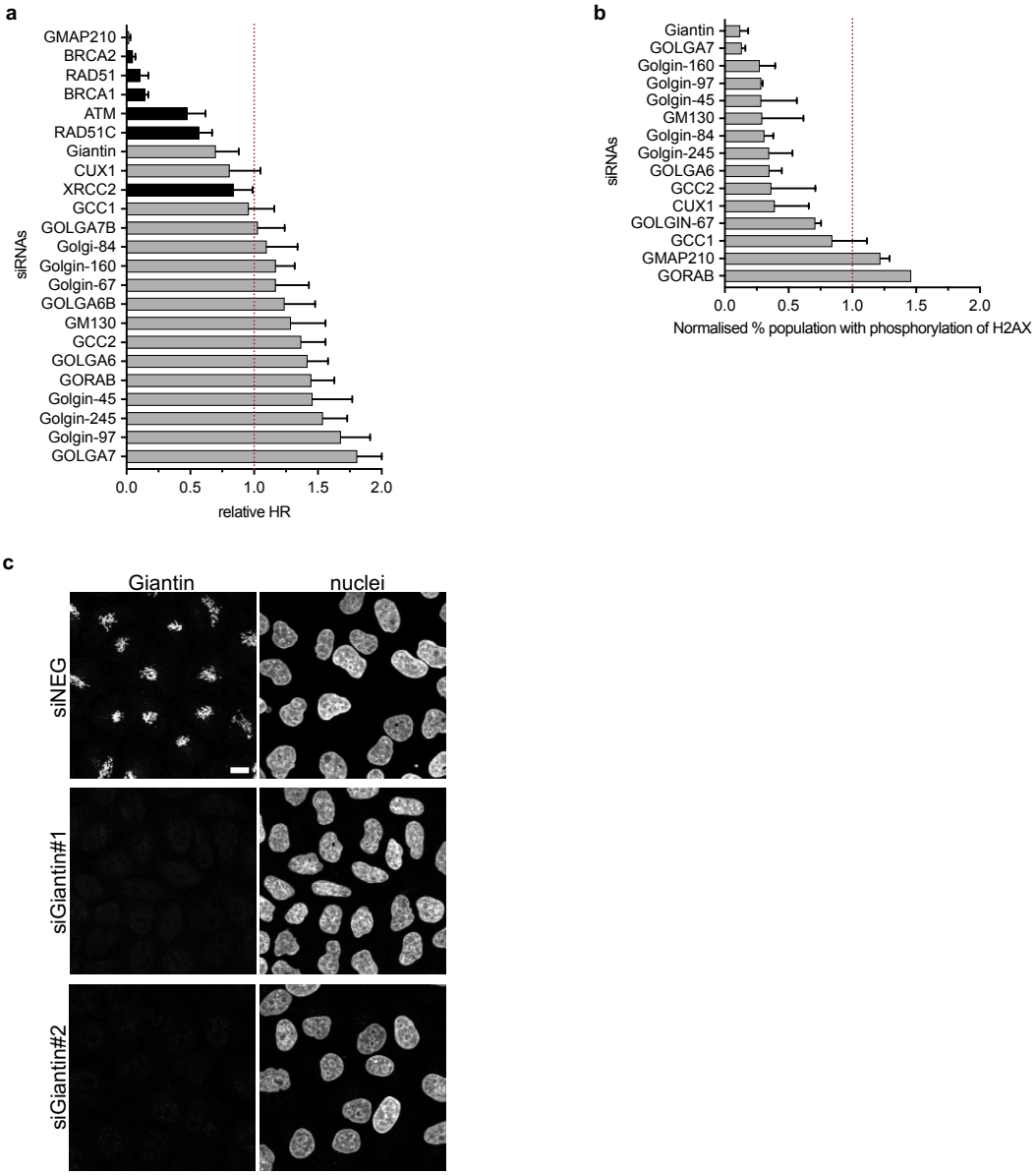

EXTENDED DATA FIGURE 4. (a) siRNA screen data (Adamson et al, 2012) showing the relative homologous recombination (HR) repair rate upon systematic knockdown of the Golgin protein family (grey) and HR complex proteins (black). (b) siRNA screen data (Paulsen et al., 2009) showing the relative percent cell population with phosphorylation of H2AX upon systematic knockdown of the Golgins. The datasets are normalised to the negative control set at 1. (c) HK cells were transfected with control, or Giantin siRNAs for 72 hours. The cells were stained with antibodies against Giantin and nuclei stained with Hoechst 33342; scale bar 10 μm.